***Date**: October 8, 2025*
Department of Translational Molecular Pathology (TMP)
Immune Profiling Laboratory
Cancer Immune Monitoring and Analysis Center
The University of Texas MD Anderson Cancer Center
TMP-Immunoprofiling (TMP-IL) Laboratory Co- Directors:
Luisa Maren Solis Soto, Associate Professor, TMP
Cara Haymaker, Associate Professor, TMP

THE UNIVERSITY OF TEXAS
MD Anderson Cancer Center
Making Cancer History®

NanoString/ Bruker GeoMx Digital Spatial Profiling Analytical Validation of Whole Transcriptome Atlas (WTA)

1. Technical platform

The GeoMx® Digital Spatial Profiling (DSP) technology is a platform developed by NanoString (Bruker). This product relies upon *in situ* hybridization probes to target around 18,000 RNA targets. The assay was validated by the manufacturer, and technical performance was evaluated using RNAseq data and RNA *in situ* hybridization. Additional details of this validation and performance can be found here (1). The assays is performed in slide-mounted tissue sections, after the incubation of RNA probes and mIF antibodies, cell types of interest can be visualized with fluorescent morphology markers for selecting region of interest (ROIs). The oligonucleotide tags are released from discrete regions of the tissue via UV exposure. Released tags are quantitated using next generation sequencing (Illumina NovaSeq 6000) and counts are mapped back to tissue location, yielding a spatially resolved digital profile of analyte abundance (2).

This document describes **verification and validation** of the **assay performance** that has been performed at the Translational Molecular Pathology Immunoprofiling Laboratory (TMP-IL). A smooth workflow and standard of operating procedures are developed by our laboratory (3)(4, 5).

2. Analytes

a. *GeoMx DSP Morphology Biomarkers for Visualization of Solid Tumor and Tumor Microenvironment:*

PanCK, CD68, CD3e, SYTO13

b. *GeoMx Human* WTA

3. Analytical characteristics

GeoMx Digital Spatial profiler platform	
Parameters	DSP target probes of the Whole Transcriptome Atlas Assay (WTA), obtained from ROIs of up to 660 um x 785 um, guided by morphological assessment of formalin-fixed paraffin-embedded (FFPE) tissue. Assay counts were subjected to quality control following manufacturer guidelines and normalized using RUVseq (6). The normalized counts were used to perform unsupervised clustering analysis, differential gene expression analysis and correlation between assay runs (***Data quality control and normalization,*** **Section 4.1**)
Accuracy	Accuracy was measured **by the capacity of the assay to accurately identify known biological compartments** in tonsil tissue (Germinal center, Interfollicular area, Mantle zone), **(Section 4.1),** mesothelioma tissue, a multi tissue microarray (TMA), and two TMAs with surgical lung adenocarcinoma (LUAD) samples using clustered dendrograms of regions of interest by gene expression patterns, **(Section 4.2 and 4.3).** Differential gene expression analysis was performed between different biological compartments of LUAD **(Section 4.3)** and tonsil tissue **(Section 4.4)** and immune cell deconvolution was performed to visualize immune cell proportions between tonsil compartments **(Section 4.5).**
Analytical sensitivity	Analytical sensitivity was measured **by the capacity of the assay to detect known differentially expressed genes in each biological compartments** of tonsil tissue. To further investigate if these patterns correspond to the biomarker expression patterns obtained with orthogonal assays, we compared the differential gene expression of selected biomarkers in biological compartments with the differential biomarker expression in tonsil tissue using protein-and RNA-based assays (Protein: single chromogenic immunohistochemistry-9 biomarkers, DSP protein-9 biomarkers; RNA: RNAscope-5 biomarkers) **(Section 5.1)**. We also correlated DSP-WTA gene expression of pleural mesothelioma and lung adenocarcinoma samples with bulk RNAseq data from the same tissue samples **(Section 5.2).** Furthermore, we evaluated if the DSP assay have the capacity to identify tissue-specific gene expression patterns concordant with specific tissue types by using a multi-tissue TMA; we evaluated a selected set of epithelial genes (KRT) and assess if the DSP-WTA assay could identify KRT associated genes in “epithelial” ROI compared to “non-epithelial” ROI **(Section 5.4.1)**. Finally, we evaluated if the expression of “tissue specific” genes had higher expression in distinct tissue types of the TMA concordant with expected higher levels of expression **(Section 5.4.2).**
Analytical specificity	Analytical specificity was measured **by the capacity of the assay to detect true negative expression** of 138 negative probes in the WTA panel compared with the rest of the RNA probes, **(Section 5.3);** In addition, we used the multi-tissue TMA and selected a set of epithelial genes (KRT) to evaluate the capacity of the assay to detect low expression of KRT genes in “non-epithelial” ROI compared to “epithelial” ROI **(Section 5.4.1)**. We also evaluated if the expression of “tissue

	specific" genes have lower expression in concordance with expected lower levels of expression in different tissue types of the TMA **(Section 5.4.2).**
Precision Inter-assay reproducibility.	Reproducibility was measured by testing three different runs, on different days and with different operators **(Section 6).**
Establishment of appropriate quality control & improvement procedures	Positive and negative controls are included in the GeoMx Human WTA assay. All the required equipment has annual service contracts with regular preventive maintenance performed to maintain optimal calibration and performance. All other small equipment and laboratory material have been calibration performed by certified vendors.

4. Accuracy

4.1 Unsupervised hierarchical clusters of gene expression data of tonsil tissue align with its biological compartments

We used a formalin fixed paraffin embedded (FFPE) tonsil tissue processed with the GeoMx DSP WTA assay to evaluate the expression of biomarkers in different biological compartments defined as: Germinal center (GC), Interfollicular area (IF), Mantle zone (MZ) and Reticulated epithelium (RE). We performed an unsupervised hierarchical cluster dendrogram to evaluate if the regions of interest (ROIs) clustered together according to their biological patterns.

Experimental Design

Samples:

-One 5µm section of FFPE with tonsil tissue.

Selection of Regions of Interest. We selected 4 to 5 ROIs placed in each biological compartment, for a total of 18 ROIs: Germinal center (GC, 4 ROIs); Interfollicular areas (IF, 5 ROIs); Mantle Zone (MZ, 5 ROIs); Reticulated Epithelium (RE, 4 ROIs) ***Figure 1A***. Placement of ROI was guided by morphology evaluation of the multiplex immunofluorescence (mIF) imaged section, performed by a pathologist.

Data quality control and normalization: FASTQ files of DSP WTA assay were processed into digital count conversion (DCC) files using GeoMx NGS pipeline (7). Quality controls of the DCC files were performed using GeoMxTools (8) package in R (version 4.2.0), R studio (9) and segments were filtered based on minimum number of reads (1000), minimum % of reads trimmed (80%), minimum % of reads stitched (80%), minimum % of reads aligned (75%), minimum sequencing saturation (50%), minimum negative control counts (1), maximum counts observed in NTC well (9000), minimum number of nuclei estimated (200), minimum segment area (1000).

Figure 1: Biological validation of WTA assay using GeoMx DSP **A.** Tonsil tissue stained with CK, CD68, CD3e and SYTO13 and illustrating regions of interest selected based in biological compartments as interfollicular area (IF), germinal center (GC), and mantle zone (MZ). **B.** Unsupervised cluster heat map of tonsil tissue showing clustering by biological compartment.

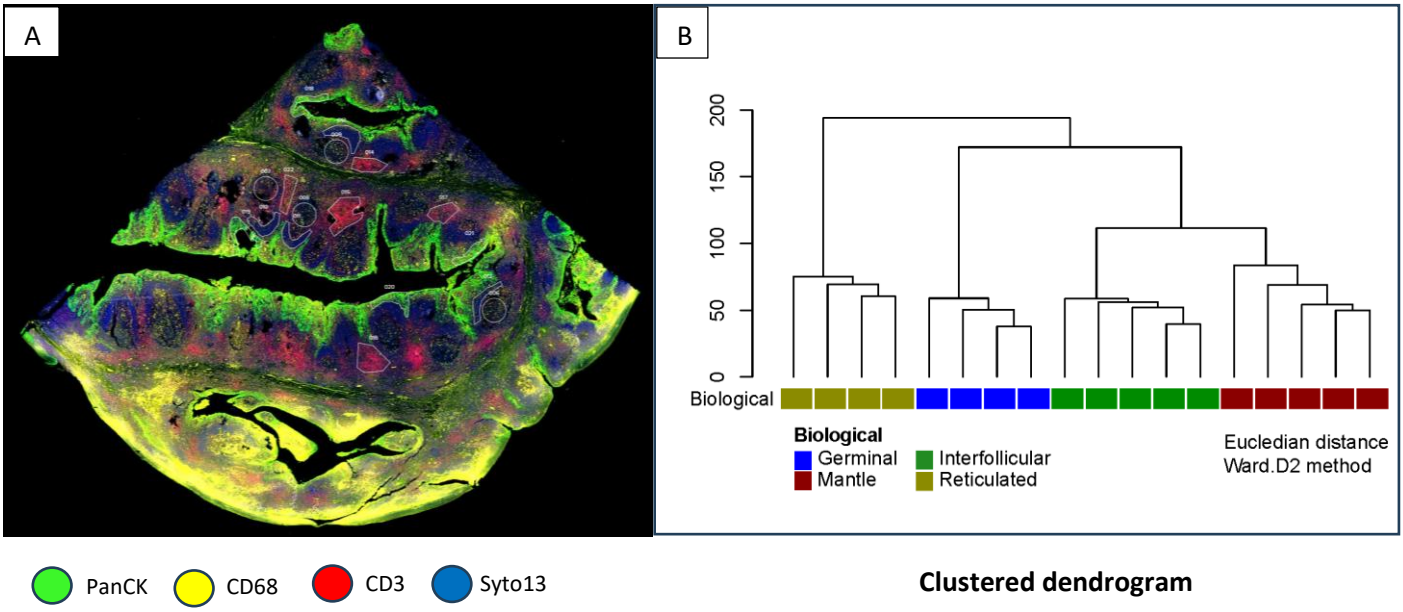

A probe was removed globally from the dataset when the geometric mean of that probe's counts from all segments divided by the geometric mean of all probe counts representing the target from all segments was less than 0.1 or the probe is an outlier according to the Grubb's test in at least 20% of the segments. Segments with less than 5% of the genes detected were removed. Qualified digital counts were normalized using RUVg normalization using housekeeping genes (*FCF1*, *DHX16*, *ABCF1*, *EDC3*, *ZNF143*, *HDAC3*, *CNOT10*, *SAP130*, *AGK*, *AMMECR1L*, *SF3A3*, *COG7*, *TMUB2*, *ZC3H14*, *DDX50*, *MRPS5*, *ZNF346*, *MTMR14*, *ERCC3*, *EIF2B4*, *TLK2*, *NUBP1*, *USP39*, *PRPF38A*, *NOL7*, *CNOT4).* (10)

Results: The clustered dendrogram showed 4 separate clusters, each cluster aligning with areas of the same distinct biological compartment (GC, IF, MZ, RE) ***Figure 1B***.

4.2 Gene expression data from multiple tissues clusters by distinct tissue type

To further investigate biological expression of genes based on tissue type, we used a formalin fixed paraffin embedded (FFPE) surgically resected pleural mesothelioma (Meso) and a multi-tissue TMA and performed a clustered dendrogram.

Experimental Design

Samples:

1) One 5µm section of an FFPE multi-tissue TMA with the following tissue types:

- Appendix
- Colorectal carcinoma
- Glioblastoma Multiforme (GBM)
- Hodgkin Lymphoma
- Liver
- Melanoma
- Pancreas
- Placenta
- Spleen
- Tonsil

2) Three serial 5µm sections of one FFPE surgical resected Mesothelioma sample.

Selection of Regions of Interest: In the multi-tissue TMA, we selected one ROI on each tissue core (total of 21 ROIs, 21 AOI) with no further segmentation in areas of illumination (AOI). In the surgical resected mesothelioma sample, we selected 8 ROIs per section identified by morphological assessment of the mIF image, the ROI were segmented into "Tumor" (PanCk+) and the surrounding tumor microenvironment "TME" (PanCk-). ROIs matched similar spatial areas in all mesothelioma slides. One slide (Meso3) had folded tissue; therefore, we only selected 5 ROI in this section (Total of 21 ROI, 42 AOI)

Results: The unsupervised clustered dendrogram showed that ROIs from tissues of the same tissue type clustered together (e.g. melanoma, mesothelioma, liver, pancreas and tonsil), indicating that the platform can capture the differential biological features by gene expression profile in a distinct tumor type. From the tissue types that had only one area, spleen and appendix sub-clustered together, Hodgkin lymphoma and placenta are in a separate cluster, and the glioblastoma (GBM) and colorectal carcinoma were individually clustered. **(Figure 2).**

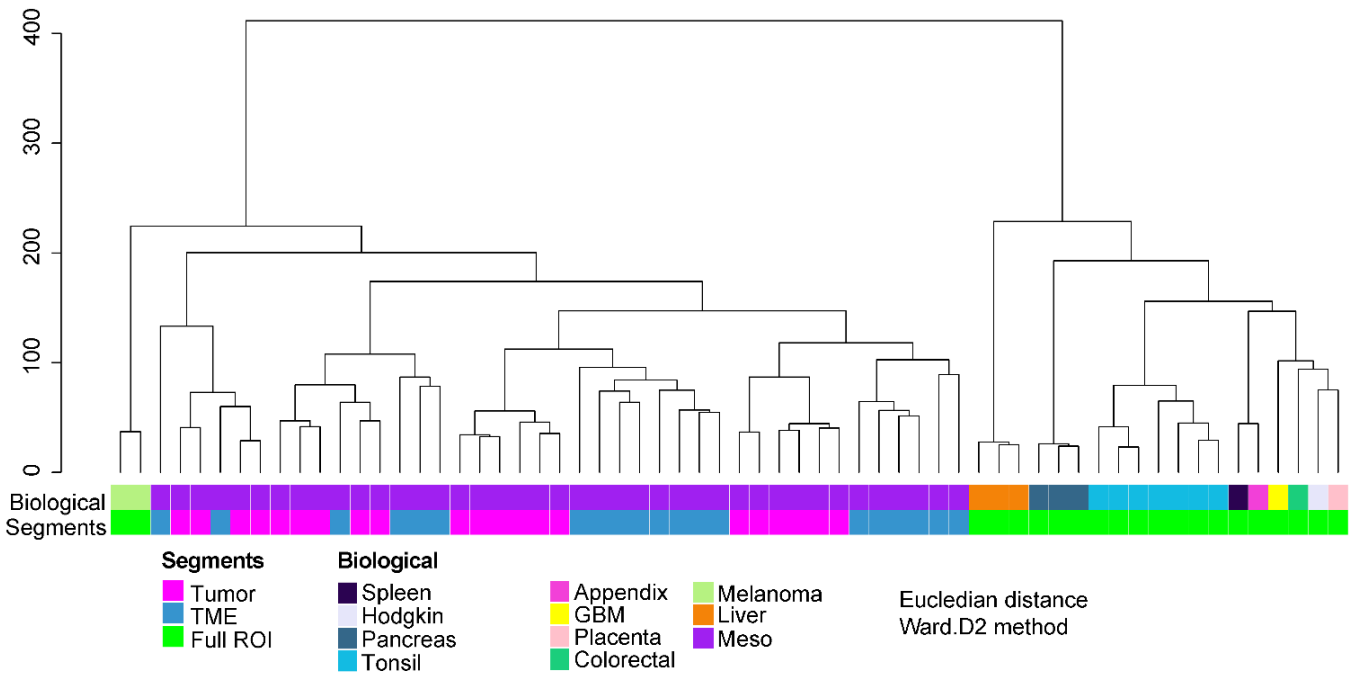

Figure 2: Unsupervised clustered dendrogram of areas of Mesothelioma and Multi-tissue TMA

4.3 Unsupervised hierarchical clusters of gene expression data of lung adenocarcinoma TMAs align with biological compartments

To further investigate if the gene expression data associates with biological compartments in independent samples, we used two FFPE TMAs containing surgically resected treatment-naïve lung adenocarcinoma samples from 33 patients with stage I/II from the MD Anderson ICON cohort(11), and evaluated the transcriptomic profile in areas with malignant epithelial cells (Tumor) and its surrounding tumor microenvironment (non-malignant epithelial cells).

Experimental Design

Samples:

-One 5µm section of FFPE with surgically resected early stages primary lung adenocarcinomas (LUAD) (Patients: 33) placed in two TMAs. The TMA was constructed with up to three tumor cores from each patient's sample obtained from the central tumor region and or invasive margin.

Selection of Regions of Interest.

We selected rectangles of 660x785 um in tumor cores with malignant cells and surrounding TME (88 cores), each ROI was segmented in Tumor (panCK+) and TME (panCK-)

Data quality control and normalization: FASTQ files of DSP WTA assay were processed into digital count conversion (DCC) files using GeoMx NGS pipeline (7). Quality controls of the DCC files were performed using GeoMxTools (8) package in R (version 4.2.0), R studio (9) and segments were filtered based on minimum number of reads (1000), minimum % of reads trimmed (80%), minimum % of reads stitched (80%), minimum % of reads aligned (75%), minimum sequencing saturation (50%), minimum negative control counts (1), maximum counts observed in NTC well (9000), minimum number of nuclei estimated (200), minimum segment area (1000). A probe was removed globally from the dataset when the geometric mean of that probe's counts from all

segments divided by the geometric mean of all probe counts representing the target from all segments was less than 0.1 or the probe is an outlier according to the Grubb's test in at least 20% of the segments. Segments with less than 5% of the genes detected were removed. Qualified digital counts were normalized using RUVg normalization using housekeeping genes (*FCF1*, *DHX16*, *ABCF1*, *EDC3*, *ZNF143*, *HDAC3*, *CNOT10*, *SAP130*, *AGK*, *AMMECR1L*, *SF3A3*, *COG7*, *TMUB2*, *ZC3H14*, *DDX50*, *MRPS5*, *ZNF346*, *MTMR14*, *ERCC3*, *EIF2B4*, *TLK2*, *NUBP1*, *USP39*, *PRPF38A*, *NOL7*, *CNOT4) (10).*

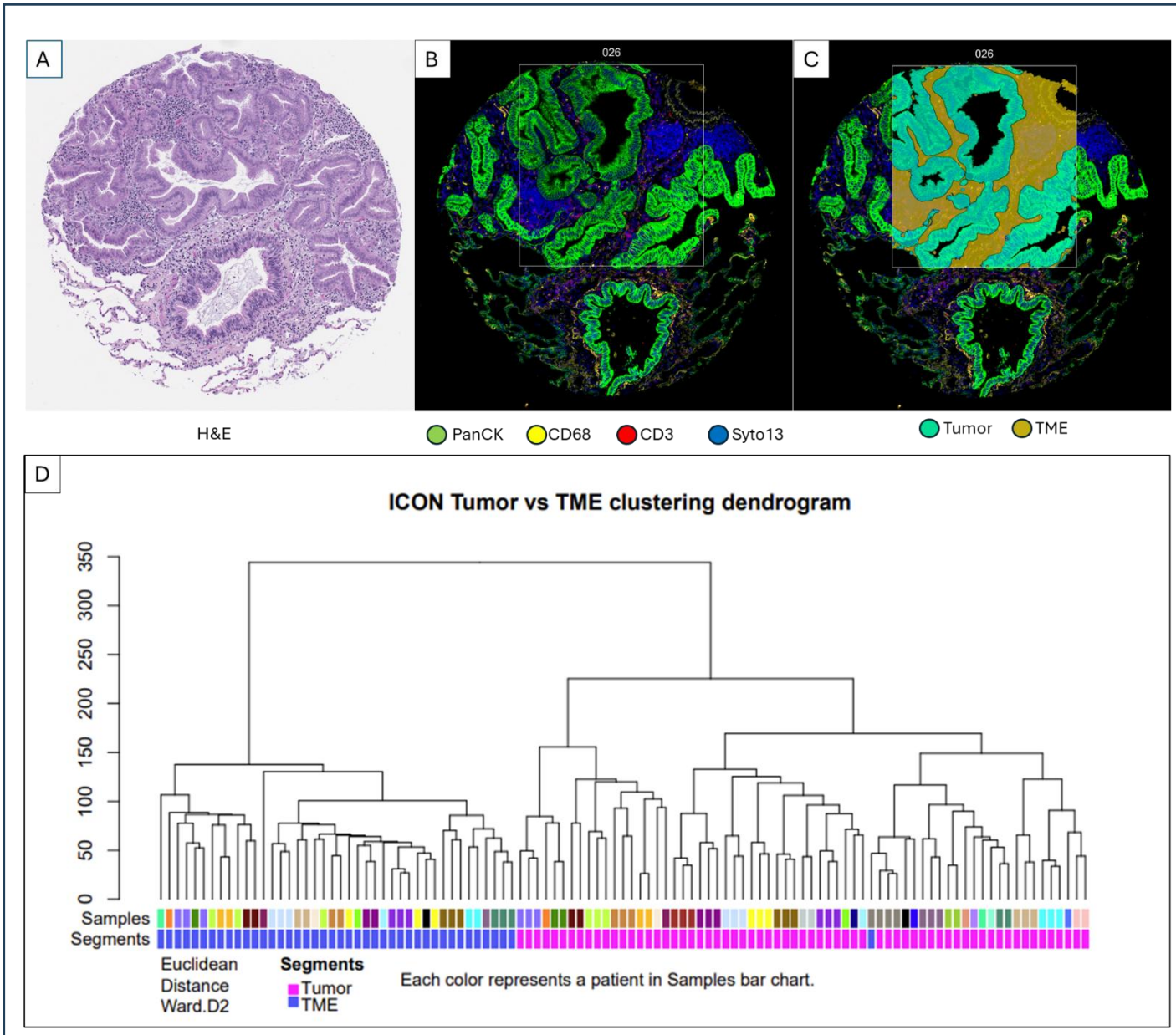

Figure 3: Microphotographs of a TMA core with Lung adenocarcinoma stained with H&E **(A),** DSP multiplex immunofluorescence **(B)** and the DSP segmentation mark-up **(C).** Unsupervised clustered dendrograms of gene expression data of the lung adenocarcinoma TMA **(D)**

Results: Unsupervised hierarchical clustering dendrogram of LUAD TMAs showed two distinct cluster branches. TME segments were clustered separately from Tumor segments which recapitulate the biological knowledge. **(Figure 3)**. The DGE profile of the tumor areas showed overexpression of genes associated with epithelial lineage (e.g. *EPCAM, KRT7, KRT8)* among others, while the TME showed expression of genes expected to be expressed in the TME such as genes associated to immune (e.g. *IGHG1, IGHG4*) or stroma (e.g. *COL1A2, COL3A1, VIM*) **Figure 4** .

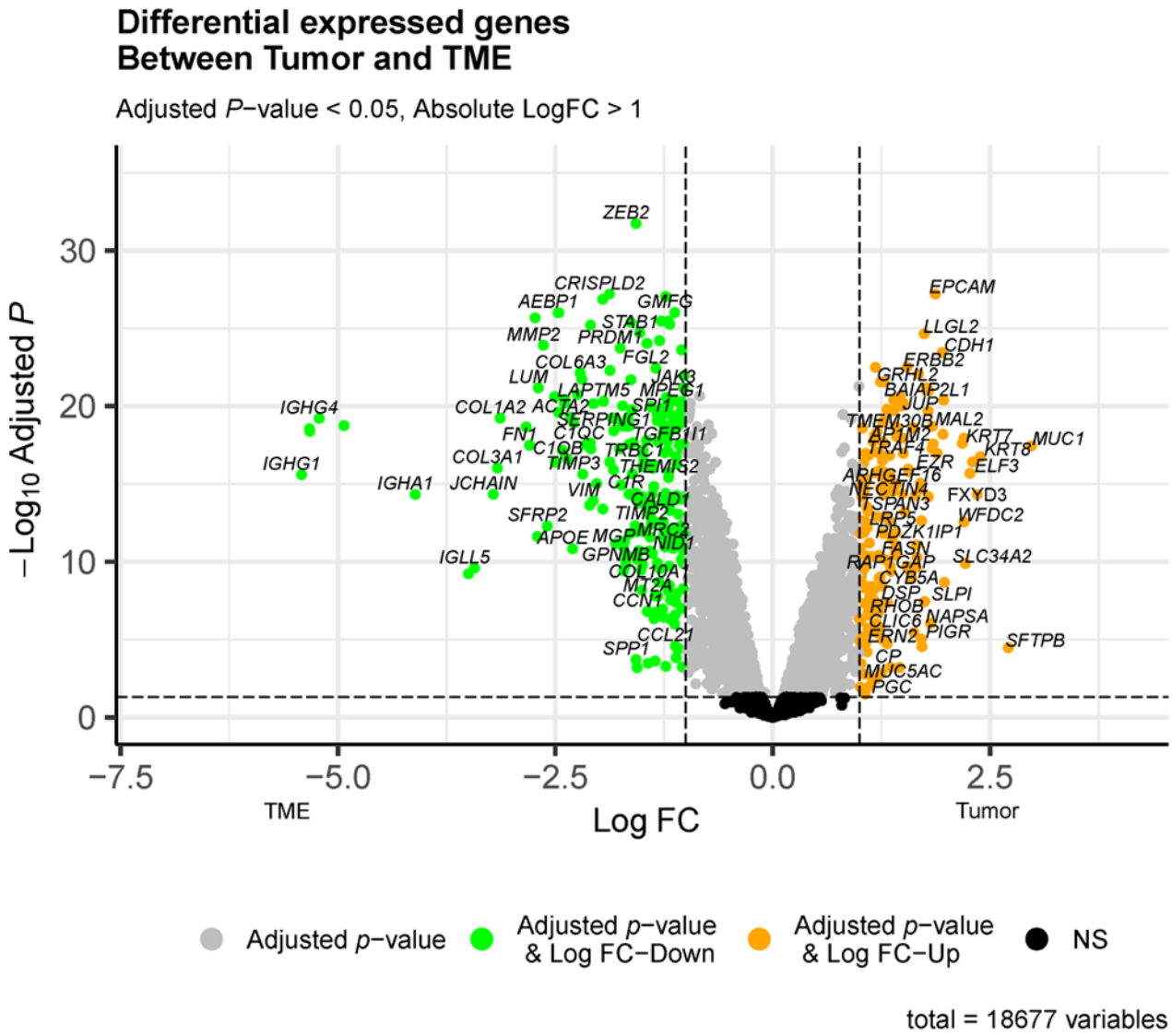

Figure 4. Differentially gene expression analysis between Tumor and the tumor microenvironment (TME) of lung adenocarcinoma samples

4.4 Differentially expressed genes in tonsil tissue biological compartments

To evaluate if the platform can distinguish distinct gene expression patterns based on biological compartments, we performed a differential expression of genes on the tonsil tissue segments: GC Vs IF, GC Vs MZ, GC Vs RE, IF Vs MZ, IF Vs RE, MZ Vs RE.

Experimental Design

Samples: Three 5µm section of FFPE tonsil tissue samples.

ROI selection strategy: ROIs of biological compartments (GC, IF, MZ, RE)

Data analysis: Normalization was performed using RUVg normalization using housekeeping genes. Differentially expressed genes (DEGs) were identified after normalization; p-values were corrected for multiple hypothesis with Benjamini-Hochberg (BH) (12) adjustment.

Results: We found differentially expressed genes between biological compartments using a Log2 Fold change > 1 and < -1 and an adjusted p value (BH) of ≤ 0.05. We reviewed if the differential expressed genes were related to known cellular components of each biological compartment. We found that genes related to T-cells were differentially expressed in IF areas (e.g. *CD8A*, *CD3E*, *CD3D, CD4*), genes related to germinal center activity (e.g. *NUGGC*, *SERPINA9*, *MYBL2, BCL6*) in GC areas, genes related to mantle B cells (e.g. *CD69*, *CD72*, *CD19*, *CD79A*, *PAX5, BANK1*) in MZ, and genes associated to epithelial cells (e.g. *KRT5*, *KRT14*, *KRT6A*) were differentially expressed in RE. **Table 1** showed selected DEG genes that are biologically associated to tonsil biological compartments.

GC Vs IF		GC Vs MZ		GC Vs RE		IF Vs MZ		IF Vs RE		MZ Vs RE	
GC	IF	GC	MZ	GC	RE	IF	MZ	IF	RE	MZ	RE
IRF6	*CCL21*	*RGS13*	*FCMR*	*YY1*	*EGFR*	*TNFRSF8*	*CR2*	*S100A4*	*EGFR*	*ALOX5*	*S100A9*
IRF4	*CCL19*	*NUGGC*	*FCER2*	*IRF4*	*ERBB2*	*IL10RA*	*IGHM*	*TNFRSF1B*	*ERBB2*	*CCR6*	*KRT5*
NFKB1	*CCR7*	*MEF2B*	*CXCL13*	*NFKB1*	*ERBB3*	*CXCR3*	*CD22*	*FOXP3*	*ERBB3*	*IGHM*	*S100A8*
NFKBIE	*IL7R*	*MYBL1*	*BANK1*	*CD19*	*KRT1*	*FOXP3*	*CD79A*	*CCR5*	*KRT10*	*CD79A*	*KRT14*
PRDM1	*CD7*	*MYBL2*	*IL16*	*FOXO1*	*KRT10*	*CCR5*	*MS4A1*	*CD4*	*KRT13*	*CD19*	*KRT6A*
TCF3	*CD8A*	*BCL6*	*CD19*	*MZB1*	*KRT13*	*GZMA*	*CD79B*	*TNFRSF8*	*KRT14*	*BANK1*	*MSLN*
CD19	*KLRK1*	*SERPINA9*	*BCL6B*	*MS4A1*	*KRT14*	*TNFRSF1B*	*ALOX5*	*CXCR3*	*KRT15*	*MS4A1*	*KRT13*
CD40	*CD3E*	*MZB1*	*PLAC8*	*CD40*	*KRT15*	*S100A4*	*MZB1*	*NKG7*	*KRT16*	*PAX5*	*KRT16*
CD79B	*CD3D*	*TCF3*	*CCR6*	*CD79A*	*KRT16*	*NKG7*	*CXCL13*	*GZMA*	*KRT17*	*CD79B*	*KRT19*
PAX5	*LAG3*	*PRDM1*	*COL19A1*	*TCF3*	*KRT17*	*CCL5*	*FCER2*	*CCR4*	*KRT18*	*CD72*	*KRT15*
MZB1	*CD247*	*CR2*	*LFNG*	*PAX5*	*KRT18*	*GZMK*	*CD19*	*LAG3*	*KRT19*	*FCMR*	*S100A14*
CD79A	*NKG7*	*CD79A*	*S1PR1*	*CD79B*	*KRT19*	*CCR4*	*BANK1*	*GZMB*	*KRT2*	*CD22*	*MALL*
BCL6	*CD44*	*YY1*	*SELL*	*BCL6*	*KRT2*	*KLRG1*	*CCR6*	*CCL5*	*KRT23*	*CR2*	*KRT80*
MYBL2	*CD2*	*PAX5*	*C12orf42*	*SERPINA9*	*KRT23*	*GNLY*	*FCMR*	*CD248*	*KRT4*	*FCER2*	*ERBB2*
MYBL1	*CCL5*	*NFKB1*	*ABCB4*	*CR2*	*KRT3*	*CD248*	*CD72*	*KLRG1*	*KRT5*	*CXCL13*	*KRT4*
SERPINA9	*CD8B*	*CD79B*	*CD69*	*MYBL2*	*KRT38*	*CD40LG*	*PAX5*	*CD40LG*	*KRT6A*	*POLRMT*	*KRT17*
NUGGC	*GZMK*	*CD40*	*RASGRP2*	*MYBL1*	*KRT4*	*LAG3*	*FDCSP*	*GZMK*	*KRT7*	*EIF4A2*	*EGFR*
MEF2B	*GZMB*	*IRF4*	*PARP15*	*NUGGC*	*KRT5*	*IDO1*	*TCL1A*	*CTLA4*	*KRT76*	*SF3B1*	*KRT78*
FOXO1	*GNLY*	*H3C12*	*LARGE2*	*MEF2B*	*KRT6A*	*CTLA4*	*NCF1*	*CD8A*	*KRT78*	*ZC3H7A*	*KRT2*
YY1	*IDO1*	*H1-5*	*LUM*	*RGS13*	*KRT7*	*GZMB*	*VPREB3*	*KLRK1*	*KRT8*	*DELE1*	*KRT8*
MS4A1	*GZMA*	*H3C2*	*GAPT*	*NOC2L*	*KRT72*	*CD4*	*COL19A1*	*CD2*	*KRT80*	*USP19*	*ERBB3*
CR2	*CXCR3*	*H3C3*	*P2RY10*	*REXO4*	*KRT73*	*CD2*	*TNFRSF13C*	*IL7R*	*MALL*	*GDI1*	*MUC15*
RGS13	*CD248*	*H3C15*	*LCN10*	*THUMPD1*	*KRT76*	*CD8A*	*CLEC17A*	*CD247*	*MSLN*	*MAP3K7*	*KRT18*

Table 1: Selected differentially expressed genes when comparing biological compartments from tonsil. These genes are related to biological compartments of GC (Cell proliferation), IF (T cell), RE (Epithelium) and MZ (B cell).

4.5 Immune cell deconvolution further identifies immune cell populations based on tissue tonsil compartments

We evaluated if WTA data could estimate proportions of immune cell populations in each biological compartments of tonsil tissue, we performed gene deconvolution to identify proportions of 22 immune subtypes.

Experimental Design

Samples: Three serial 5µm section of FFPE tonsil tissue samples.

ROI selection strategy: ROIs of biological compartments (GC, IF, MZ, RE)

Data analysis: Normalization was performed using RUVg normalization using housekeeping genes. CIBERSORTx (13) and SpatialDecon (14) deconvolution methods were performed.

Results: Using both deconvolution methods, we found higher proportions of naïve B cells in GC and MZ, and plasma cells in GC, which is concordant to B-cell stages of differentiation in the tonsil tissue; macrophages M0 (non-polarized macrophages) (CIBERSORTx) and macrophages (SpatialDecon) were found at higher proportions in the RE, while M2 macrophages (polarized macrophages) (CIBERSORTx) were found at higher proportions in IF and GC. T-cell subtypes were observed at higher proportions in the IF areas, with the expected exception of the T cell follicular helper (CIBERSORTx) with higher proportion in the GC . NK cells (SpatialDecon) and resting and activated NK cells (CIBERSORTx) have higher proportions in the RE (activated) and in the IF (resting) region. These findings overall align with expected patterns of immune cell proportions in tonsil tissue compartments.

We found some differences in proportions between these two deconvolution methods, briefly memory B cells were higher in the MZ, RE and GC using CIBERSORTx while the proportions of memory B cells identified with SpatialDecon were lower in the GC and MZ; of note, memory cells are expected to be present in GC and epithelium of tonsils (15). Also, monocytes (CIBERSORTx) have higher proportions in the IF area while monocytes (non-classical, NC, and intermediate, I; CIBERSORTx) have higher proportions in the RE and IF area; classical monocytes (CIBERSORTx) have overall very low proportions in all compartments. Neutrophils identified by SpatialDecon seem to have higher proportions in the RE while neutrophils identified by CIBERSORT have overall lower proportions in all compartments The differences in the cell type and proportions seem to be driven by the differences in reference matrix; CIBERSORTx was run using LM22 reference matrix (13) while the SpatialDecon was run using SafeTME matrix (14). It is advisable to use a reference library customized for each tumor type to better deconvolute this data. **(Figure 5 and Figure 6)**.

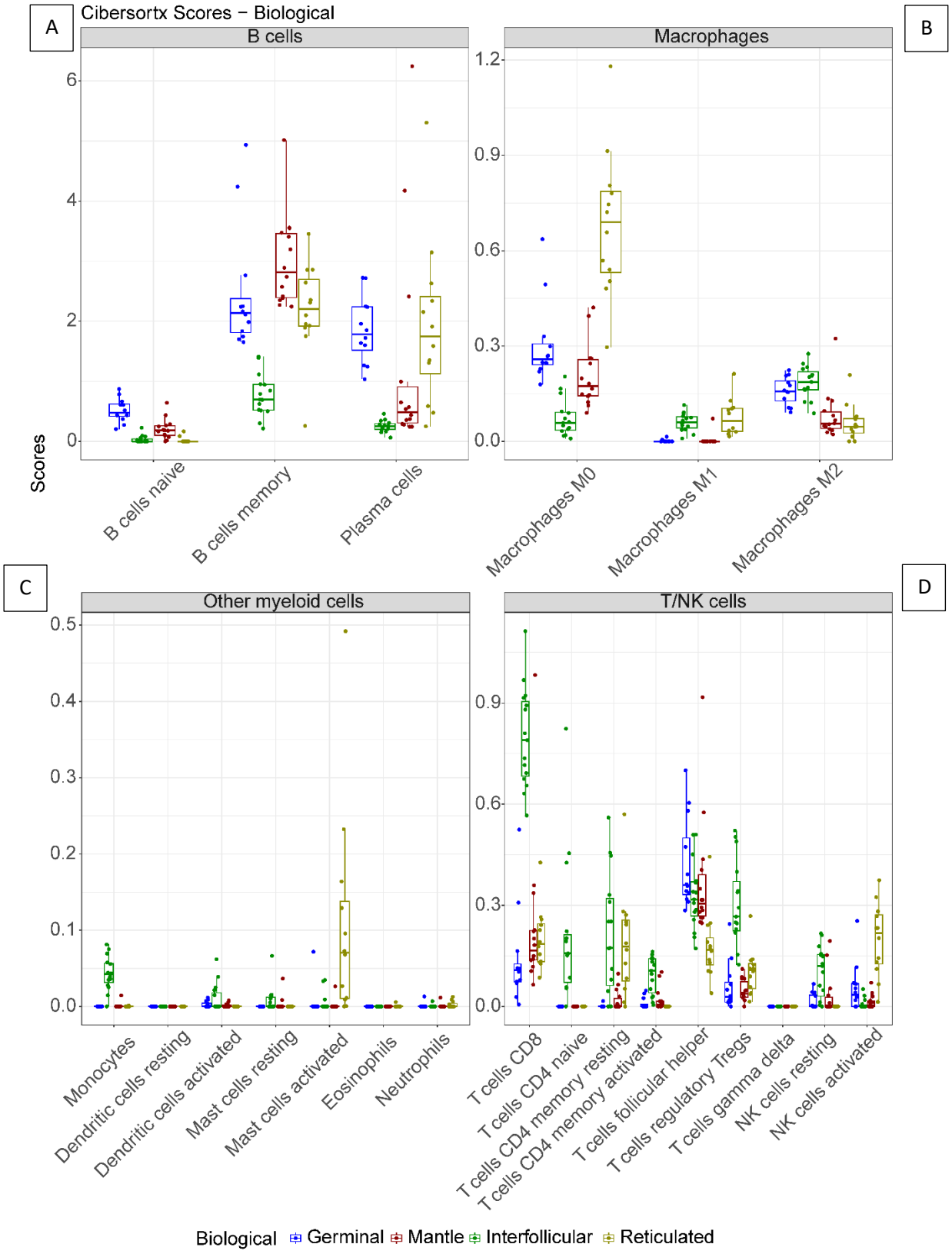

Figure 5: Immune cell deconvolution using CIBERSORTx showing proportion of cells in the different biological areas of A) B cells B) Macrophages, C) Myeloid cells (non-macrophages) D) T and NK cells.

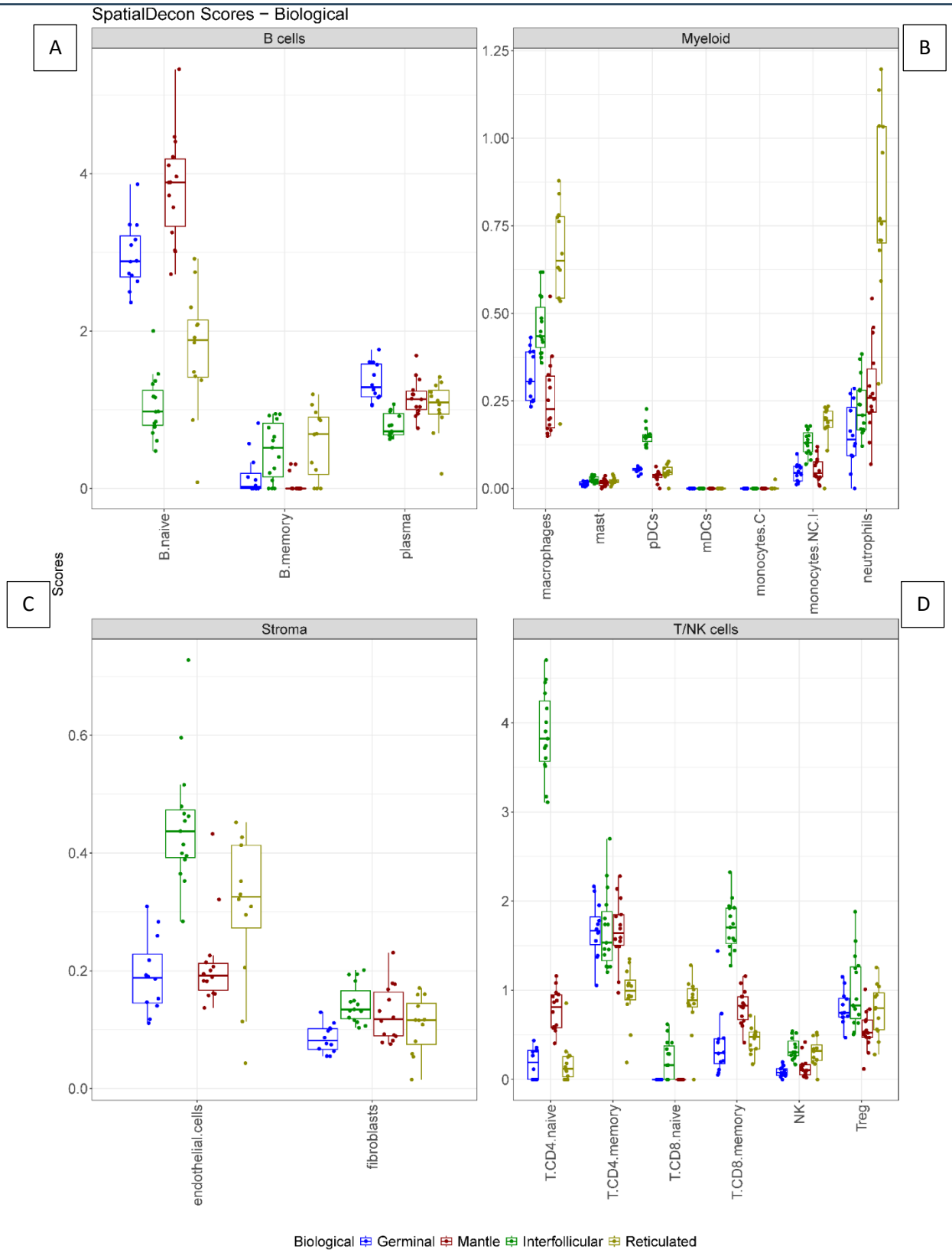

Figure 6: Immune cell deconvolution using Spatialdecon showing proportion of cells in the different biological areas of A) B cells B) Myeloid, C) Stroma D) T and NK cells.

5. Analytical Sensitivity and specificity

5.1 Orthogonal platform comparison of tonsil tissue gene expression with RNAscope and protein platforms

To evaluate analytical sensitivity of the WTA counts, we compared WTA RNA expression of a group of genes, on the same biological tonsil tissue compartments (GC, IF, MZ and RE), with annotated information of gene and protein expression of those biomarkers using orthogonal platforms for protein [Single chromogenic Immunohistochemistry (IHC) and the DSP GeoMx protein assay] and RNA (RNAscope) expression. Details of the biomarkers for each platform can be seen in **Table 2**.

Experimental Design

Samples:

1. For DSP WTA: Three serial 5µm section of a FFPE tonsil tissue sample.
2. For IHC*: 5µm sections (n=11) of a FFPE tonsil tissue sample stained with IHC antibodies.
3. For DSP Protein*: 5µm section of a FFPE tonsil tissue sample.
4. For RNAscope#: 5µm section of a FFPE tonsil tissue sample stained with RNAscope probes.

ROI selection strategy: *For DSP WTA,* ROIs of biological compartments (GC, IF, MZ, RE) matched in the three serial sections.

Data analysis: Normalization was performed using **RUVg** normalization using housekeeping genes. Boxplots were elaborated using "R" and "GraphPad" software to visualize gene and protein expressions.

*For IHC and DSP Protein, ROI selection, image analysis and data normalization were described in the **NanoString GeoMx Digital Spatial Profiling Analytical Validation of Immuno-oncology Protein Targets** (16). Of note, for IHC we used the percentage of tissue with positive expression of the biomarker, for DSP-protein, we used normalized DSP counts.

For RNAscope, ROI selection and image analysis were described in the **Analytical Validation of RNAscope Assay for Immuno-oncology Biomarker Probes**(17) . Of note, for RNAscope, we used the average optical density of the ROI.

Results: We observed similar patterns of expression of biomarkers associated to T cells (CD3E, CD4 and CD8A), myeloid cells (CD163, CD14), B cells (CD20), and proliferation (Ki67), between DSP WTA genes and IHC and DSP-protein. Briefly, in all platforms, T cell biomarkers (*CD3E, CD4* and *CD8A*) have higher expression in IF areas compared to GC and MZ, while B cell biomarker (CD20) was higher in GZ and MZ compared to IF area. *CD163* was higher in the IF areas while *CD14* was higher in the GC compared to IF and MZ. Ki67 showed higher expression in GC. In addition, KRT8 and *KRT18* genes had higher expression in epithelial cells, like the pattern of panCK by IHC. PD-L1 expression data was also available by IHC, DSP and RNAscope. The RE had higher expression of *CD274* gene (DSP-WTA and RNAscope) and PD-L1 (IHC) . Interestingly, PD-L1 was higher in GC compared to MZ and IF at protein level, however gene expression of *CD274* was not higher in GC compared to MZ and IF by both DSP-WTA and RNAscope. *CTLA4* had higher expression in IF areas compared to GC by DSP-WTA, RNAscope and DSP-protein while its expression was the highest in the GC using IHC. The reticulated epithelium had lower expression of *CTLA4* by DSP-WTA and IHC and higher expression by RNAscope (**Figures 7A, 7B and 7C).** *IL10* and *IFNG* showed similar levels of expression in GC, IF and RE; and TNFRSF8 (CD30) was higher in IF by DSP-WTA and IHC, but not by RNAscope. Discrepancies in gene

and protein expression in different biological compartments are expected and may be related to tissue heterogeneity, post-translational modifications, other biological processes or limitations of assay performance.

Table 2: List of genes from the WTA assay compared with genes from an RNA orthogonal platform (RNAscope) and orthogonal protein platforms immunohistochemistry (IHC) and DSP protein assays.

WTA	**RNAscope**	**IHC**	**DSP protein**
CTLA4	*CTLA4*	CTLA4	CTLA4
CD274	*CD274*	PD-L1	PD-L1
IL10	*IL10*		
IFNG	*IFNG*		
TNFRSF8	*TNFRSF8*		
CD3E		CD3	CD3
CD4		CD4	CD4
CD8A		CD8	CD8
CD14		CD14	CD14
MS4A1		CD20	CD20
ITGAX		CD11c	CD11c
CD163		CD163	CD163
MKI67		KI67	KI67
KRT8		PanCK	PanCK
KRT18		PanCK	PanCK

A

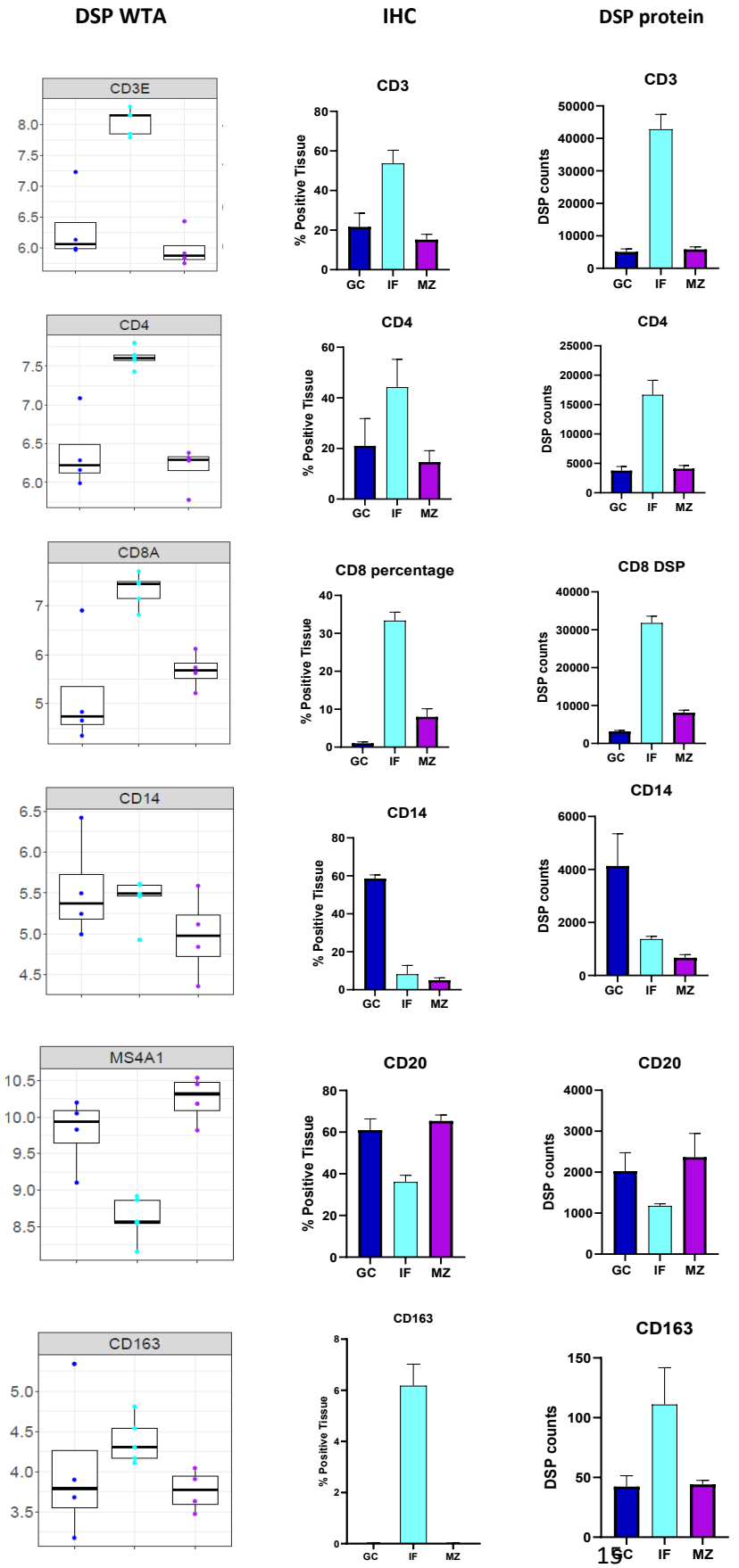

Figure 7A: Expression of DSP WTA probes in germinal center, interfollicular areas and mantle zones of tonsil tissue, compared with immunohistochemistry as percentage of positive cells, immunohistochemistry as positive tissue area and DSP protein probes, for ***CD3, CD4, CD8A, CD14, MS4A1*** **(CD20) and CD163** (GC: Germinal center, IF: Interfollicular areas, MZ: Mantle zone.)

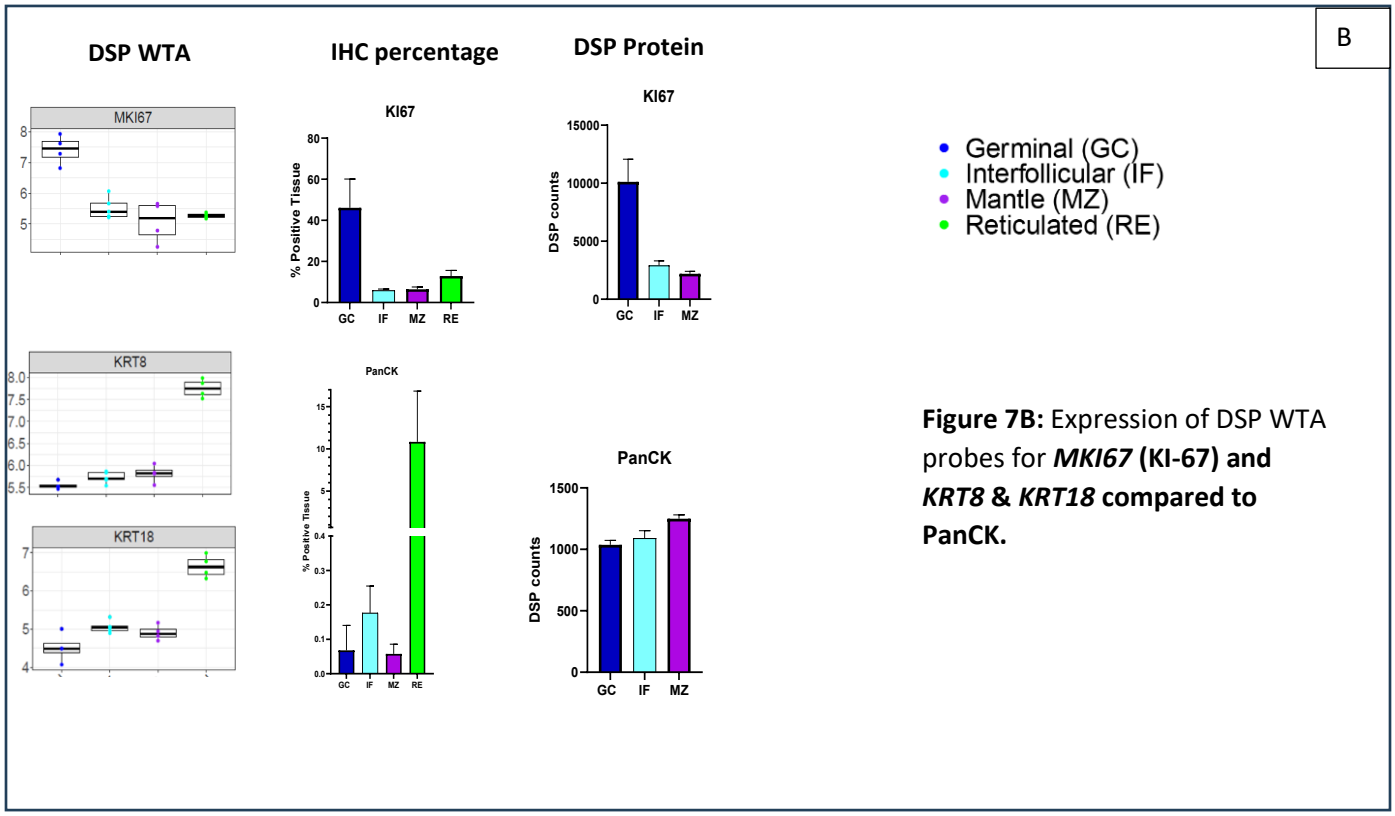

Figure 7B: Expression of DSP WTA probes for ***MKI67*** **(KI-67) and** ***KRT8*** **&** ***KRT18*** **compared to PanCK.**

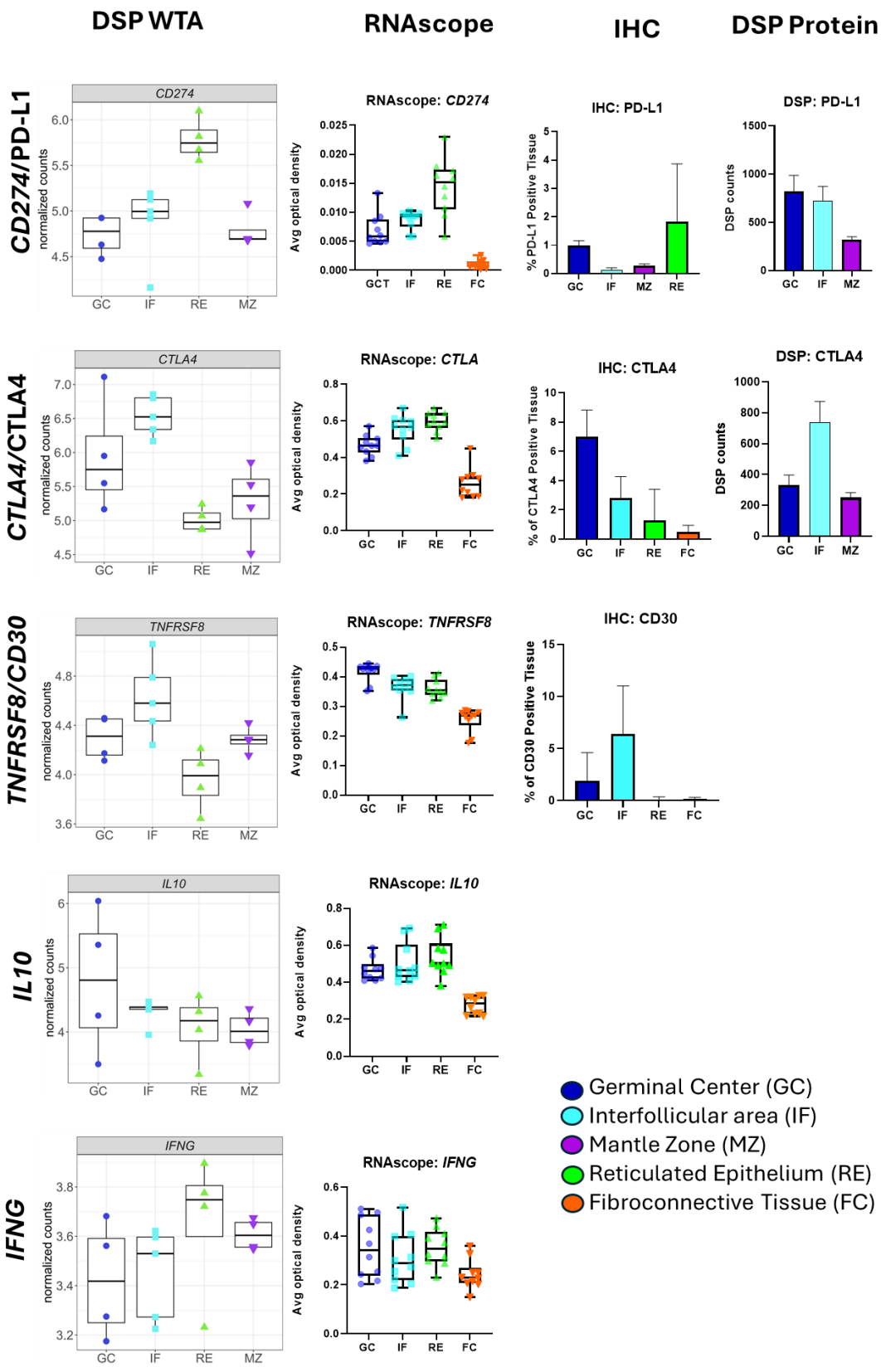

Figure 7C: Expression of DSP WTA probes compared with RNAscope, immunohistochemistry and DSP protein probes for ***CD274*** **(PD-l1),** ***CTLA4, TNFRSF8*** **(CD30),** ***IL10*** **and** ***IFNG.***

5.2 Orthogonal platform comparison of tonsil tissue gene expression with RNAseq

We also investigated the performance of the WTA panel of the GeoMx DSP assay compared to annotated data of bulk RNAseq. For this analysis, we used FFPE surgical resected mesothelioma and lung adenocarcinoma tissues with DSP-WTA gene expression data and compared it with annotated data of bulk RNAseq analysis obtained from fresh frozen tissue of the same samples.

Experimental design

Samples:

-One 5µm section of FFPE surgical resected mesothelioma tissue.

--One 5µm section of FFPE with primary lung adenocarcinomas (LUAD) placed in a TMAs.

ROI selection strategy: Up to 5 ROIs on the mesothelioma tissue identified by morphological assessment of the mIF image. ROI were segmented into “Tumor” (PanCk+) and “TME” (PanCk-).

Data analysis: We summed normalized read counts of DSP-WTA ROIs from same patient and performed log2 transformation. Log2 transformed normalized read counts of bulk RNAseq of samples that were in the DSP-WTA were used in the correlation analysis. Correlation analysis was performed with Pearson correlation in R.

Results: For the mesothelioma sample, a moderate correlation (R=0.44) was observed between WTA gene expression of 5 ROIs when compared with bulk RNAseq data **(Figure 8A).** For the lung adenocarcinoma samples from the TMA, the correlation was also moderate (R:0.42) **(Figure 8B).**

A

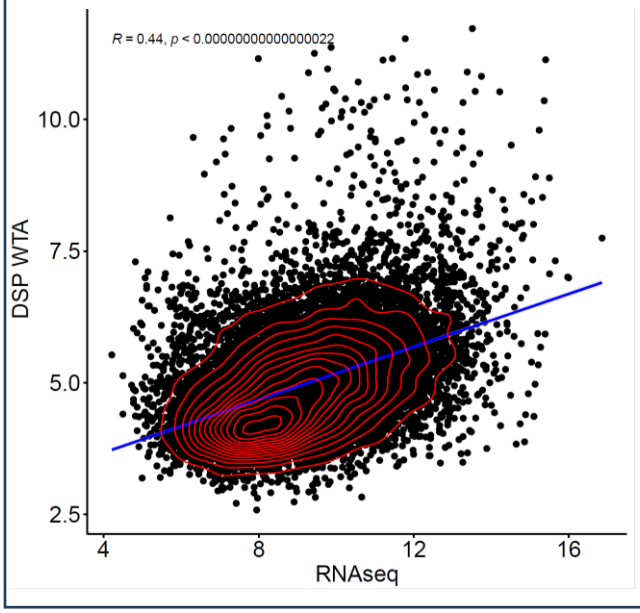

Figure 8A: Correlation of RNA probes from WTA assay **Meso sample** and bulk RNAseq obtained from the same tissue.

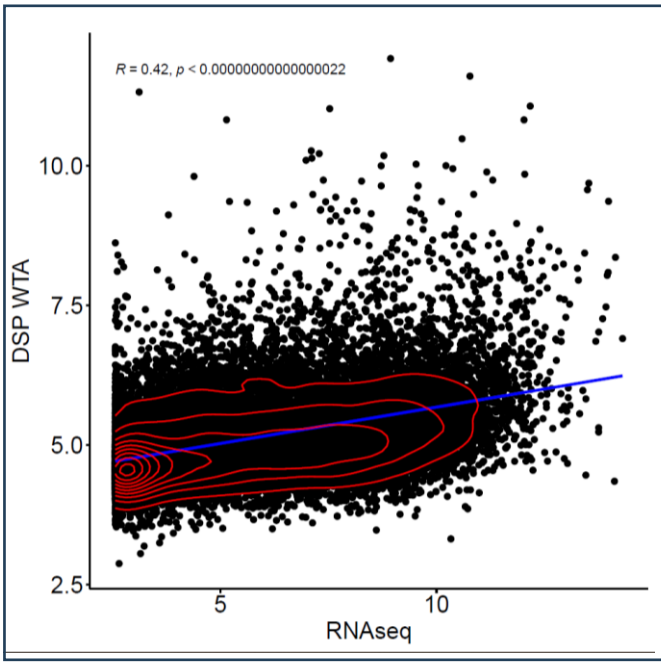

Figure 8B: Correlation of RNA probes from WTA assay **ICON samples** and bulk RNAseq obtained from the same tissues.

5.3 Evaluation of negative probes of the DSP-WTA panel.

Analytical specificity was measured by the capacity of the assay to detect true negative expression of 138 negative probes in the WTA panel compared with the rest of the RNA probes.

Experimental design:

Samples:

1) Three 5µm section of FFPE of slides containing tonsil tissue and whole tissue section of a surgical resected mesothelioma sample
2) One 5µm section of FFPE with multi-tissue TMA

Data analysis: We had 138 negative controls in the DSP-WTA assay. We combined read counts of same genes/negative controls per TMA and visualized them with ggplot2 (18) package in R.

Results:

We plotted the expression of negative probes in all the samples, compared with the expression of positive probes form the WTA assay. In this case, we were able to visualize negative probes closer to 0 (log2 of total counts) vs a wide range of positive probe expressions. Nevertheless, some genes were expressed close to the negative probe range (e.g. FNBT) **(Figure 9).** Due to this, a QC and probe filtering by percentage of expression is performed for every assay **(see *Data quality control and normalization section 4.1).***

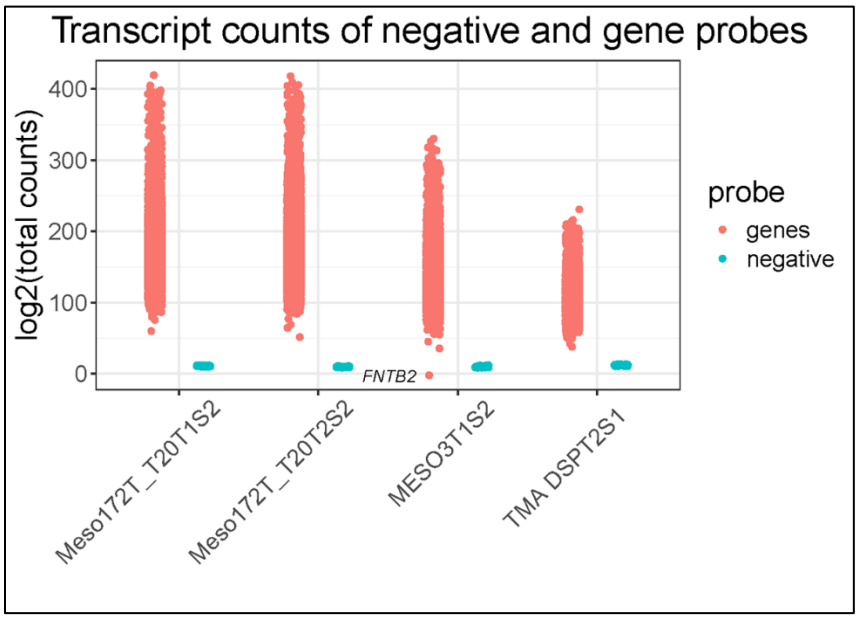

Figure 9: Comparison of probes from WTA assay including Meso samples and multi-tissue TMA.

5.4 Differential expression of genes in a multi tissue TMA (specificity and sensitivity)

To further investigate the capacity of the assay to detect low levels (specificity) or high levels (sensitivity) of biomarkers in tissue specific types, we used a multi-tissue TMA to investigate differential gene expression analysis in epithelial and non-epithelial tissue types and gene expression of tissue specific biomarkers in distinct tissue types.

5.4.1 Epithelial Vs non-epithelial tissue types.

We used a multi-tissue TMA and selected a set of epithelial genes (KRT) to evaluate the level of expression of KRT genes in “non-epithelial” ROI compared to “epithelial” ROI.

Experimental Design

Samples:

1) One 5µm section of FFPE of a multi-tissue TMA with the following samples:
- Appendix
- Colorectal carcinoma
- Glioblastoma Multiforme (GBM)
- Hodgkin Lymphoma
- Liver
- Melanoma
- Pancreas
- Placenta
- Spleen
- Tonsil

Selection of Regions of Interest: One ROI on each tissue core (total of 21 ROIs) for the TMA. Cores were categorized into “epithelial” if they showed any kind of epithelial cell present, and “non-epithelial” if they didn’t show any epithelial cells: **(Figure 10)**

- Epithelial: Appendix, colorectal carcinoma, liver, pancreas, placenta, tonsil (with superficial or reticulated epithelium).

- Non-epithelial: GBM, Hodgkin lymphoma, melanoma, spleen.

Data analysis: Differentially expressed genes (DEGs) were identified after normalization; p-values were corrected for multiple hypothesis with Benjamini-Hochberg (BH) (12) adjustment.

Figure 10: Multi-tissue TMA processed with DSP WTA and morphology markers PanCK, CD68, CD3 and Syto13 (nuclei), to evaluate differential gene expression of tissue types. A) Morphology scan showing markups for ROIs selected on the tissue cores. B) Same morphology image without the ROI markup with an example of a non-epithelial core in a white box and an epithelial core in a blue box. C) Higher magnification of non-epithelial core (spleen). D) Higher magnification of epithelial core (pancreas).

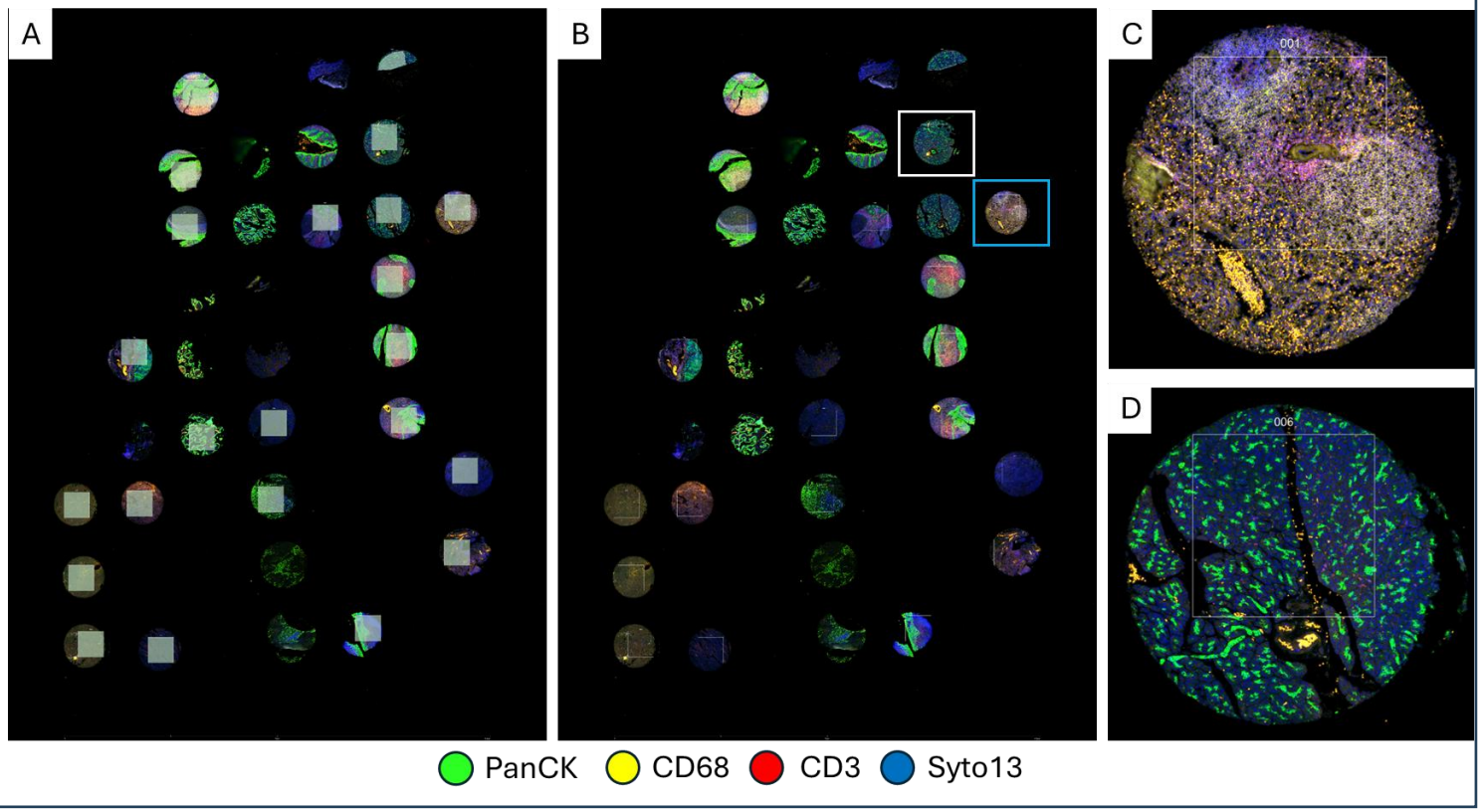

Results: We observed differential higher expression of epithelial related genes (*KRT13*, *KRT6A*, *KRT5*) in cores with epithelial cells compared to cores with non-epithelial cells (**Figure 11)**

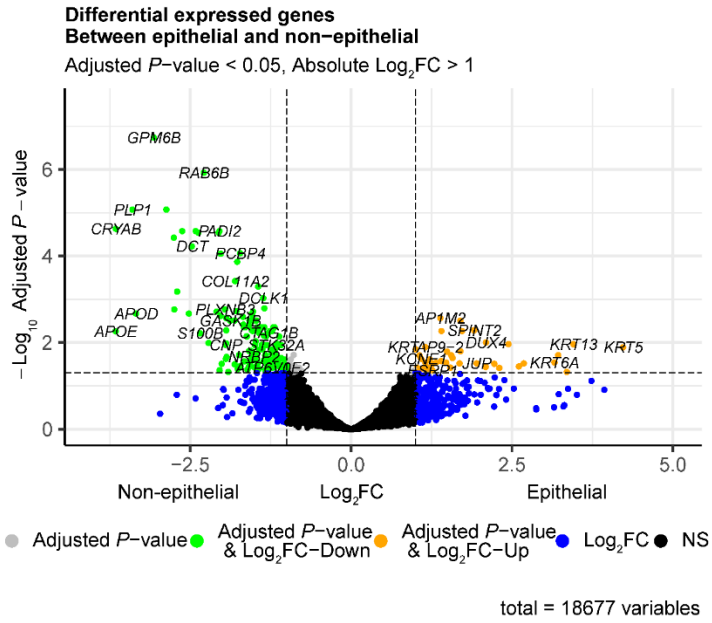

Figure 11: Differential gene expression between "epithelial and "non-epithelial" tissue cores.

5.4.2 Evaluation of tissue specific biomarkers.

To further study the differential expression of genes by tissue type, we visualized the gene expression data of a set of "tissue specific" genes and used them as positive controls of their target tissue in comparison with other tissue types.

Experimental design:

We selected "tissue specific" genes based on current literature as follows:

1) **Colorectal carcinoma:** *KRT20*(19) (CK20) and *MUC2*(20)
2) **Glioblastoma:** *GFAP(21), CD56* (NCAM1)(22)
3) **Liver:** *Arg1* (Arginase)(23)
4) **Melanoma:** *PMEL*(24)
5) **Pancreas:** *PRSS2* (Serine protease 2)(25)
6) **Mesothelioma:** *MSLN* (Mesothelin)(26)

Results: Selected genes showed higher expression in the target tissue when compared to the rest of the tissue types **(Figure 12).**

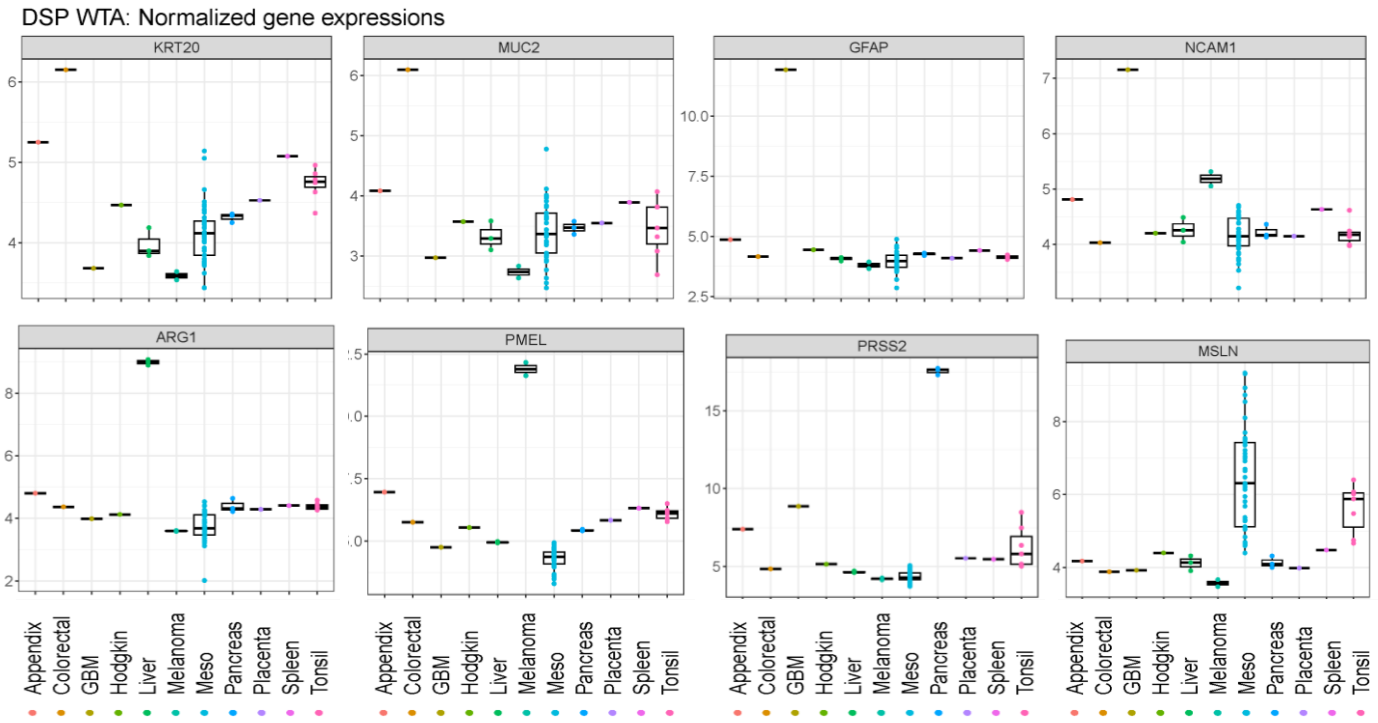

Figure 12: Comparison of expression of "tissue specific" genes in different tissue types (Appendix, Colorectal carcinoma, Glioblastoma, Hodgkin lymphoma, Liver, Melanoma, Mesothelioma, pancreas, spleen and tonsil).

6 Reproducibility of biological validation results

To investigate reproducibility of the assay, we performed two independent tests at separate times:

1) **Test 1, day 1:** One slide with tonsil tissue and a Meso tissue.
2) **Test 2, six weeks apart**: Two consecutive slides with tonsil tissue and Meso tissue. In this case, both slides were scanned and processed at the same time.

For both tests, we replicated biological areas using the same strategy for ROI selection and ROI segmentation.

6.1 Intra run reproducibility

To test reproducibility of results in the same run, we performed a correlation between the 2 slides from test 2.

Experimental design

Samples: Three 5µm section of FFPE with tonsil tissue and Meso tissue.

ROI selection strategy: We placed up to 5 ROIs on each tonsil biological compartment (GC, IF, MZ, RE) and 5 ROIs on the Meso tissue identified by morphological assessment of the mIF image. Meso areas were segmented into "Tumor" (PanCk+) and "TME" (PanCk-). ROIs matched similar spatial areas in all slides.

Data quality control and normalization: Normalization was performed using RUVg normalization using housekeeping genes. A Pearson correlation was performed.

Results:

Using all the ROIs for analysis, Test 2 slides showed a strong positive correlation **(Figure 13A).** Furthermore, a correlation was performed by different biological compartments from Meso (Tumor and TME) **(Figure 13B and 13C)** and tonsil tissue **(Figure 13D),** showing a strong correlation (R^2>0.8 with p value < 0.05) for all slide segments (mesothelioma and tonsil), Tumor segments from mesothelioma, and all segments form tonsil tissue. For the TME segments from the mesothelioma, a moderate correlation was observed (R^2 of 0.67 with p value of less than 0.05).

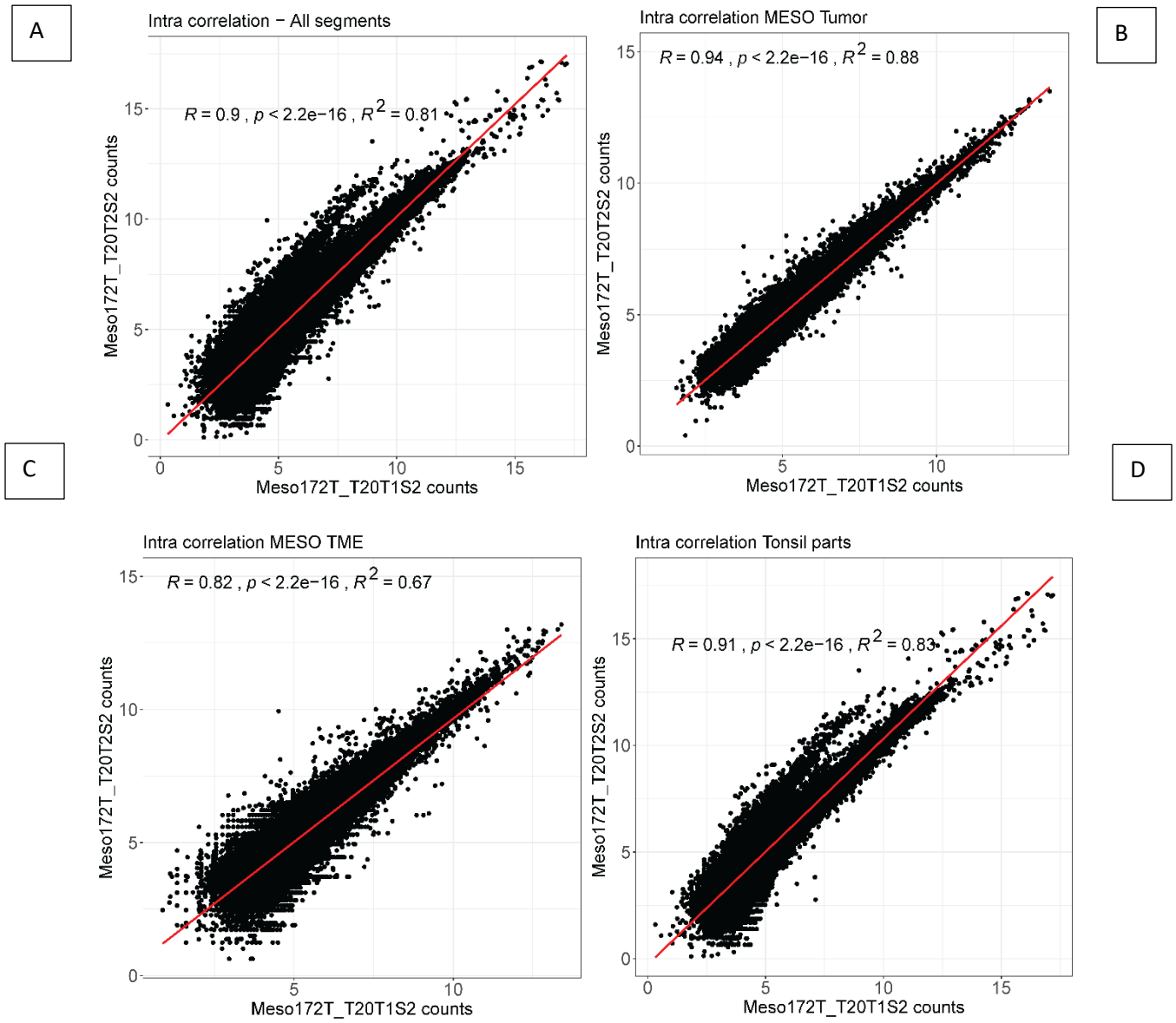

Figure 13: Intra-run reproducibility results from correlations of Test 2 slides **(A).** Correlations by different biological compartments from Meso (Tumor and TME) **(B and C)** and tonsil tissue **(D),** showing a moderate to strong correlation between samples.

6.2 Inter run reproducibility:

To test reproducibility of results in different runs, we performed a correlation between the slide from Test 1 and the slides from Test 2 as described in section 6 above.

Experimental design

Samples: Three 5µm sections of FFPE with tonsil tissue and Meso tissue.

ROI selection strategy: We placed up to 5 ROIs on each tonsil biological compartment (GC, IF, MZ, RE) and 5 ROIs on the Meso tissue identified by morphological assessment of the mIF image. Meso areas were segmented into "Tumor" (PanCk+) and "TME" (PanCk-). ROIs matched similar spatial areas in all slides.

Results: Test 1 slide showed a strong positive correlation when compared to both slides of Test 2. (**Figure 14**). To further analyze, segments were sub-grouped based on biological areas into: Tonsil, Meso-tumor and Meso-TME, obtaining a moderate to strong correlation (R^2>0.7 with p value < 0.05) between the areas of Test 1 and Test 2 slides (**Figure 15**)

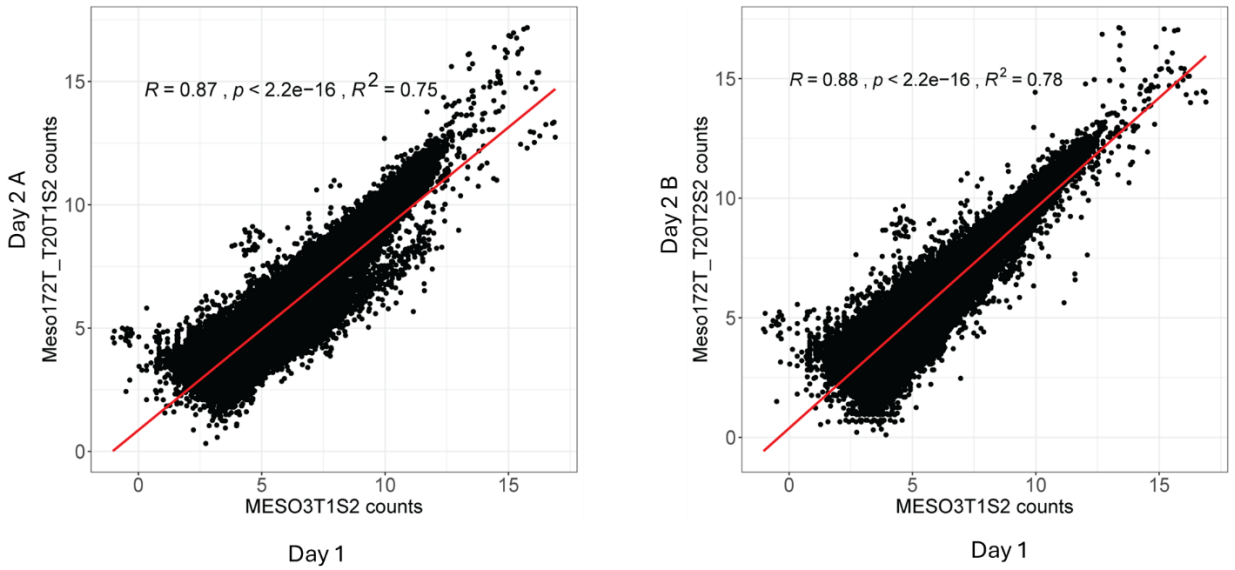

Figure 14: Inter-run correlation between the slides from Day 1 and the 2 slides processed 6 weeks apart (Day 2A and Day 2B respectively)

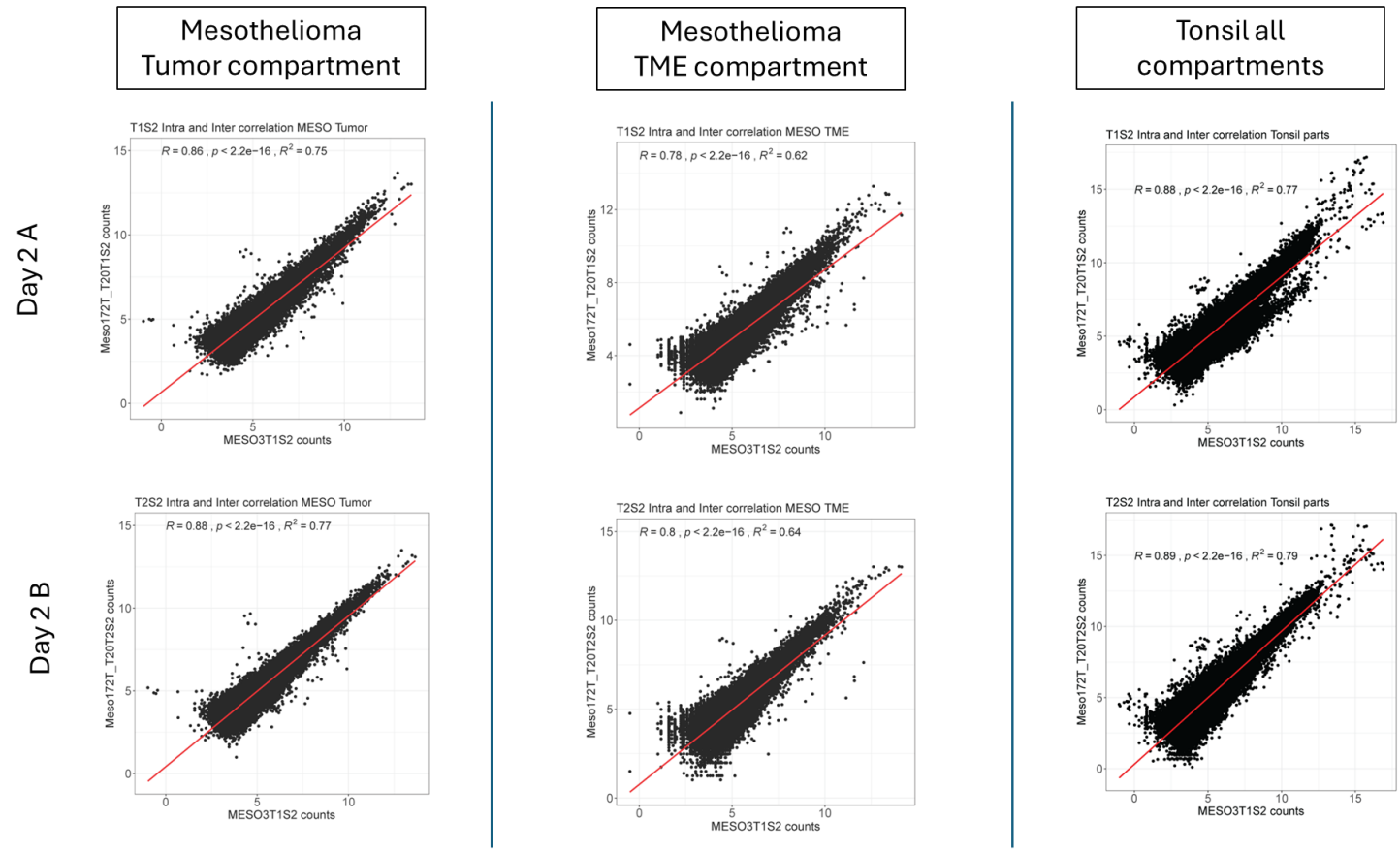

Figure 15: Inter-run correlation between the slides from Day 1 and the 2 slides processed 6 weeks apart (Day 2A and Day 2B respectively), separated by compartments of the Mesothelioma (Tumor and TME) and the compartments of the tonsil.

Conclusion

In conclusion, our data indicates that the biomarker expression of targets included in the Whole Transcriptome Atlas assay of the GeoMx DSP platform are concordant with biological patterns observed in tonsil tissue controls and multi-tissue TMA. Differential gene expression and immune cell deconvolution proportions were concordant to tonsil compartments. Gene expression of GeoMx DSP assay and orthogonal platforms (immunohistochemistry, DSP-protein and RNAscope) were similar when compared using levels of expression in biological compartments of the tonsil. Negative target probes and positive versus negative counts of specific genes in different types of tissues showed were used to show specificity. We also observed high reproducibility among runs at different run times.

Immunohistochemistry and Digital pathology Laboratory

GeoMx DSP scientist leads:

Wei Lu, MD, PhD Principal scientist.

Sharia Hernandez, MD, Sr. Research scientist.

Alejandra Serrano, MD Research scientist

Computational Biology leads:

Ken Chen, PhD, Professor.

Nejla Ozirmak Lermi, Associate data scientist

Director: Luisa Maren Solis Soto, MD Associate Professor MD Anderson Cancer Center

Signature (Luisa M. Solis Soto) **Date: 10/08/2025**

References:

1. Zimmerman SM, Fropf R, Kulasekara BR, Griswold M, Appelbe O, Bahrami A, et al. Spatially resolved whole transcriptome profiling in human and mouse tissue using Digital Spatial Profiling. Genome Res. 2022;32(10):1892-905.
2. Van TM, Blank CU. A user's perspective on GeoMxTM digital spatial profiling. Immuno-Oncology Technology. 2019;1:11-8.
3. Hernandez S, Lazcano R, Serrano A, Powell S, Kostousov L, Mehta J, et al. Challenges and Opportunities for Immunoprofiling Using a Spatial High-Plex Technology: The NanoString GeoMx((R)) Digital Spatial Profiler. Front Oncol. 2022;12:890410.
4. Database NCIBBR. Spatial transcriptomics: GeoMx Digital Spatial Profiler (DSP) nCounter Protein Assay SOP (MD Anderson) 2024 [Available from: https://brd.nci.nih.gov/brd/sop/show/3270.
5. Database NCIBBR. Spatial transcriptomics: SOP for Pathological Assessment and Region of Interest Selection using the NanoString GeoMx Digital Spatial Profiler (MD Anderson) [Available from: https://brd.nci.nih.gov/brd/sop/show/3271.
6. Risso D, Ngai J, Speed TP, Dudoit S. Normalization of RNA-seq data using factor analysis of control genes or samples. Nat Biotechnol. 2014;32(9):896-902.
7. GeoMx® DSP NGS Readout MAN-10153-06. 2024.
8. Griswold M ON, Yang Z, Vitancol R, Henderson D. GeomxTools: NanoString GeoMx Tools. 2024 [Available from: https://bioconductor.org/packages/GeomxTools.
9. RStudio: Integrated Development Environment for R [Internet]. 2025. Available from: http://www.posit.co/.
10. Chan CW, Wong NA, Liu Y, Bicknell D, Turley H, Hollins L, et al. Gastrointestinal differentiation marker Cytokeratin 20 is regulated by homeobox gene CDX1. Proc Natl Acad Sci U S A. 2009;106(6):1936-41.

11. Ozirmak Lermi N, Molina Ayala M, Hernandez S, Lu W, Khan K, Serrano A, et al. Comparison of imaging based single-cell resolution spatial transcriptomics profiling platforms using formalin-fixed paraffin-embedded tumor samples. Nat Commun. 2025;16(1):8499.
12. Benjamini Y, Hochberg Y. Controlling the False Discovery Rate: A Practical and Powerful Approach to Multiple Testing. Journal of the Royal Statistical Society Series B (Methodological). 1995;57(1):289-300.
13. Newman AM, Steen CB, Liu CL, Gentles AJ, Chaudhuri AA, Scherer F, et al. Determining cell type abundance and expression from bulk tissues with digital cytometry. Nat Biotechnol. 2019;37(7):773-82.
14. Danaher P, Kim Y, Nelson B, Griswold M, Yang Z, Piazza E, et al. Advances in mixed cell deconvolution enable quantification of cell types in spatial transcriptomic data. Nat Commun. 2022;13(1):385.
15. Palm AE, Henry C. Remembrance of Things Past: Long-Term B Cell Memory After Infection and Vaccination. Front Immunol. 2019;10:1787.
16. Database NCIBBR. Spatial transcriptomics: NanoString GeoMx Digital Spatial Profiling Analytical Validation of Immuno-oncology Protein Targets (MD Anderson) 2024 [Available from: https://brd.nci.nih.gov/brd/sop/show/3105.
17. Database NCIBBR. RNAscope: Analytical Validation of RNAscope Assay for Immuno-oncology Biomarker Probes (MD Anderson) 2024 [cited 2025. Available from: https://brd.nci.nih.gov/brd/sop/show/3265.
18. Valero-Mora PM. ggplot2: Elegant Graphics for Data Analysis. Journal of Statistical Software, Book Reviews. 2010;35(1):1 - 3.
19. Chan CWM, Wong NA, Liu Y, Bicknell D, Turley H, Hollins L, et al. Gastrointestinal differentiation marker Cytokeratin 20 is regulated by homeobox gene CDX1. Proceedings of the National Academy of Sciences. 2009;106(6):1936-41.
20. Raynaud CM, Jabeen A, Ahmed EI, Hubrack S, Sanchez A, Sherif S, et al. MUC2 expression modulates immune infiltration in colorectal cancer. Frontiers in Immunology. 2025;Volume 15 - 2024.
21. Ahmadipour Y, Gembruch O, Pierscianek D, Sure U, Jabbarli R. Does the expression of glial fibrillary acid protein (GFAP) stain in glioblastoma tissue have a prognostic impact on survival? Neurochirurgie. 2020;66(3):150-4.
22. Balik V, Mirossay P, Bohus P, Sulla I, Mirossay L, Sarissky M. Flow Cytometry Analysis of Neural Differentiation Markers Expression in Human Glioblastomas May Predict Their Response to Chemotherapy. Cellular and Molecular Neurobiology. 2009;29(6):845-58.
23. Yan BC, Gong C, Song J, Krausz T, Tretiakova M, Hyjek E, et al. Arginase-1: a new immunohistochemical marker of hepatocytes and hepatocellular neoplasms. Am J Surg Pathol. 2010;34(8):1147-54.
24. Zhang S, Chen K, Liu H, Jing C, Zhang X, Qu C, et al. PMEL as a Prognostic Biomarker and Negatively Associated With Immune Infiltration in Skin Cutaneous Melanoma (SKCM). J Immunother. 2021;44(6):214-23.
25. Witt H, Sahin-Tóth M, Landt O, Chen JM, Kähne T, Drenth JP, et al. A degradation-sensitive anionic trypsinogen (PRSS2) variant protects against chronic pancreatitis. Nat Genet. 2006;38(6):668-73.
26. Yeo D, Castelletti L, van Zandwijk N, Rasko JEJ. Hitting the Bull's-Eye: Mesothelin's Role as a Biomarker and Therapeutic Target for Malignant Pleural Mesothelioma. Cancers (Basel). 2021;13(16).